Editors' Suggestion

Viscotaxis: Microswimmer Navigation in Viscosity Gradients

Benno Liebchen,[1,*] Paul Monderkamp,[1] Borge ten Hagen,[2] and Hartmut Löwen[1]
[1]*Institut für Theoretische Physik II: Weiche Materie, Heinrich-Heine-Universität Düsseldorf, D-40225 Düsseldorf, Germany*
[2]*Physics of Fluids Group and Max Planck Center Twente, Department of Science and Technology, MESA+ Institute, and J. M. Burgers Centre for Fluid Dynamics, University of Twente, 7500 AE Enschede, The Netherlands*

(Received 23 December 2017; published 15 May 2018)

The survival of many microorganisms, like *Leptospira* or *Spiroplasma* bacteria, can depend on their ability to navigate towards regions of favorable viscosity. While this ability, called *viscotaxis*, has been observed in several bacterial experiments, the underlying mechanism remains unclear. We provide a framework to study viscotaxis of biological or synthetic self-propelled swimmers in slowly varying viscosity fields and show that suitable body shapes create viscotaxis based on a systematic asymmetry of viscous forces acting on a microswimmer. Our results shed new light on viscotaxis in *Spiroplasma* and *Leptospira* and suggest that dynamic body shape changes exhibited by both types of microorganisms may have an unrecognized functionality: to prevent them from drifting to low viscosity regions where they swim poorly. The present theory classifies microswimmers regarding their ability to show viscotaxis and can be used to design synthetic viscotactic swimmers, e.g., for delivering drugs to a target region distinguished by viscosity.

DOI: 10.1103/PhysRevLett.120.208002

Introduction.—The ability to adapt their motion in response to gradients in an external stimulus, called *taxis* [1], is crucial for the life of most microorganisms. Chemotaxis [2], for example, allows microorganisms to find food (chemoattraction or positive chemotaxis) and to escape from toxins (chemorepulsion or negative chemotaxis) but also acts as a precondition of mammalian life by guiding sperm cells towards the egg. Very recently, it was found that chemotaxis even plays an important role [3–10] in synthetic colloidal microswimmers [11–13], where it can induce dynamic clusters and patterns even at low density [4–8]. Besides responding to chemical stimuli, many biological and synthetic swimmers can adapt their motion also in response to other stimuli such as gradients in light intensity (phototaxis) [14–18], magnetic fields (magnetotaxis) [19–21], temperature (thermotaxis) [22–25], or a gravitational potential (gravitaxis) [26–31].

In this Letter we consider *viscotaxis*, which is a different kind of taxis caused by viscosity gradients. Viscotaxis is much less understood than the above types of taxes for microorganisms and is undiscovered for synthetic swimmers. However, viscosity gradients occur in many situations, both for biological and synthetic swimmers. The interface between two immiscible liquids of different viscosity, for example, features a high viscosity gradient, occurring, e.g., in a sedimentation profile of the two liquids. Similarly, viscosity gradients show up naturally in complex environments, e.g., in fluids near a mucus zone or at the interface of different parts of the human body with individual viscosities. Therefore, some microorganisms, like *Spiroplasma* [32] and *Leptospira interrogans* [33–35], which are poor swimmers at low viscosity [33,36], have developed the ability to navigate up viscosity gradients. Without this ability to perform viscotactic motion, they would statistically migrate down the gradient [36], as the residence time of a particle in a certain volume element decreases with its speed. Despite the existence of a series of experiments on bacterial viscotaxis [32,34–36], there is no systematic theory or understanding of the precise mechanism allowing microorganisms to perform viscotaxis [35]. We therefore develop a framework to study viscotaxis for self-propelled biological and synthetic microswimmers in slowly varying viscosity fields. The present approach shows that *nonuniaxial* body shapes *automatically* lead to viscous torques aligning linear swimmers *generically* up viscosity gradients. This is due to a systematic mismatch of viscous forces acting on different body parts of the swimmer. The proposed mechanism may help to explain experiments observing positive viscotaxis in *Spiroplasma* [32] and *Leptospira* [33–35], which has previously been attributed to the speculative existence of viscoreceptors [36]. The provided theory may also help linking the characteristic motility mode in *Spiroplasma* and *Leptospira*, which involves uniaxial and nonuniaxial body shapes [32,35,37–39], with the very fact that these organisms show viscotaxis [34,35]. We also demonstrate that swimmers experiencing nonviscous torques, like chiral swimmers or run-and-tumble bacteria, can, in principle, generate negative viscotaxis, which may shed new light on corresponding observations for *E. coli* bacteria [36]. More generally, our theory classifies swimmers, based on their body shape and self-produced torques, regarding their ability to perform viscotaxis. This classification can be used as a new design principle for synthetic microswimmers that are able to navigate in viscosity gradients.

Passive particles in viscosity gradients.—To develop a first understanding for the dynamics in viscosity gradients, we consider a passive and overdamped rigid body which is confined to two dimensions (quasi 2D) and consists of N rigidly connected spheres with midpoints $\mathbf{r}_i = (x_i, y_i)$ $(i = 1, \ldots, N)$ and radii b_i. Besides external forces $\mathbf{F}_i$, which we will later replace with effective self-propulsion "forces" [40–42], the spheres also experience viscous forces. Since we are mainly interested in slowly varying viscosity fields, in the sense that viscous forces do not change much on the scale of a single sphere $[|\eta(y_i + b_i) - \eta(y_i)|/\eta(y_i) \ll 1]$, we apply Stokes's law to define the frictional forces $\mathbf{F}_R(\mathbf{r}_i) \approx -6\pi\eta(\mathbf{r}_i)b_i\dot{\mathbf{r}}_i$ [for physical effects due to large viscosity gradients (discontinuities), see Ref. [43]]. This leads us to the following equations of motion:

$$\sum [\mathbf{F}_i - 6\pi b_i \eta(\mathbf{r}_i)\dot{\mathbf{r}}_i] = \mathbf{0}, \tag{1}$$

$$\sum (\mathbf{r}_i - \mathbf{R}) \times [\mathbf{F}_i - 6\pi b_i \eta(\mathbf{r}_i)\dot{\mathbf{r}}_i] = 0, \tag{2}$$

representing force- and torque-balance conditions. Here, $\mathbf{a}\times\mathbf{b} = a_1 b_2 - a_2 b_1$, $\sum := \sum_{i=1}^{N}$, and $\mathbf{R} = (X, Y)$ is some reference point for which we choose, for convenience, the hydrodynamic center of mass $\mathbf{R} := \sum b_i \mathbf{r}_i / \sum b_i$; characteristically, forces acting at this point do not cause rotations of the rigid body in the lab frame. We focus here on linear viscosity profiles $\eta(\mathbf{r}) = \eta_0 + \lambda y$, and we eliminate η_0 by shifting the origin of the coordinate system $y \to y - \eta_0/\lambda$ and λ by defining a rescaled radius $a_i = 6\pi\lambda b_i$.

To get an initial idea about the dynamics of particles in viscosity gradients, we consider externally forced bodies, say, the "sedimentation" of a sphere experiencing a constant force $\mathbf{F}_1 = F_0\mathbf{e}_y$ pointing up the gradient [Fig. 1(a)]. For a single sphere, Eqs. (1) and (2) yield $y_1(t) = y_1(t=0) + \sqrt{2F_0 t/a_1}$ and $x_1(t) = x_1(t=0)$, showing that the sphere continuously slows down as $\dot{y}_1 \propto 1/\sqrt{t}$.

While more complicated N-body objects experiencing forces $\mathbf{F}_i = F_i\mathbf{e}_y$ feature a more involved short-time dynamics, at late times, they universally follow the same $\sqrt{t}$ law as the single sphere. To see this, we write, for later convenience, $\mathbf{r}_i = \mathbf{R} - l_i\mathbf{e}_i$ [cf. Fig. 1(d)], where $l_i = |\mathbf{r}_i - \mathbf{R}|$ and $\mathbf{e}_i = (\cos\phi_i, \sin\phi_i)$, with $\phi_i =: \phi + \alpha_i$ being the angle between $\mathbf{R} - \mathbf{r}_i$ and the x axis and ϕ defining the orientation of the swimmer based on the orientation of $\mathbf{R} - \mathbf{r}_1$ relative to the x axis [Figs. 1(c) and 1(d)]. For $Y \gg l_i$, we have $y_i = Y - l_i\sin\phi_i \approx Y$ so that Eq. (1) yields $(\sum a_i)Y\dot{Y} = \sum F_i$, resulting in $Y(t) = \sqrt{2t(\sum F_i)/(\sum a_i)}$. Solving Eqs. (1) and (2) numerically, using a Runge-Kutta integrator with Dormand-Prince adaptive step-size control, for a sphere, a symmetric dumbbell, and a triangular swimmer confirms this law [see Fig. 1(b)]. Note that nonlinear viscosity profiles lead to a qualitatively analogous behavior [44].

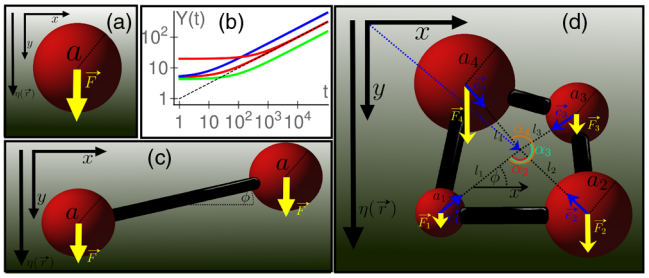

FIG. 1. The sedimentation of (a) a sphere, (c) a dumbbell, and (d) more complex objects in a linear viscosity profile $\eta(y) = \eta_0 + \lambda y$ (illustrated by the shading of the background color) universally follows (b) a $Y(t) \propto \sqrt{t}$ law at late times, where Y is the y component of the hydrodynamic center of mass [the long blue arrow in (d)]. (b) shows the sedimentation dynamics based on numerical integration of Eqs. (1) and (2) of a single sphere [the two (red) curves which merge corresponding to two different initial Y values], a symmetric dumbbell (blue, top curve at late times), and an irregular triangle (green, lower curve) (using arbitrary parameters). The black dashed line shows the $y(t) = \sqrt{t}$ line for comparison.

Conversely to the position $\mathbf{R}(t)$, the late-time orientation of a sedimenting body in a viscosity gradient depends on its shape. To see this, let us consider a symmetric dumbbell with equal forces $\mathbf{F} = F\mathbf{e}_y$ acting on the two spheres [Fig. 1(c)] and ask how it will align to the gradient while falling. To find the answer, we use the late-time solution of Eq. (1): $(X^*, Y^*) = (X(t=0), 2\sqrt{tF/(a_1 + a_2)})$, and we determine the fixed points of Eq. (2) as $\phi^* = 0,\ \pi/2$, representing the horizontal and vertical dumbbell orientations, respectively. Performing a linear stability analysis of these fixed points shows that the vertical configuration is always unstable, whereas the horizontal one ($\phi^* = 0$) attracts $\phi(t)$, which makes the dumbbell fall horizontally. Physically, for $\phi \neq 0$ the drag acting on the lower sphere [Fig. 1(c)] dominates such that the upper sphere moves faster and the dumbbell turns towards the horizontal configuration (see also movie 1 in the Supplemental Material (SM) [45]).

Microswimmer viscotaxis.—We now turn to our key aim of exploring the mechanism allowing microswimmers to navigate in viscosity gradients. Analogously to the previous considerations for externally forced passive bodies, we describe active microswimmers as multibead rigid bodies [46–48,52–55]; since our key results will apply to arbitrarily complex arrangements of (very small) beads, the model can also be used to closely mimic swimmers with a continuous shape. For clarity and generality of the physical discussion, we implement activity by effective propulsion forces [42,56], but we show in the SM [45] that equivalent results can also be derived for swimmers where the self-propulsion is explicitly modeled by body shape deformations, for example. The latter type of swimmers experience only minor corrections from hydrodynamic interactions (see the SM [45]). The effective forces point in fixed directions in the body frame of the particle and corotate

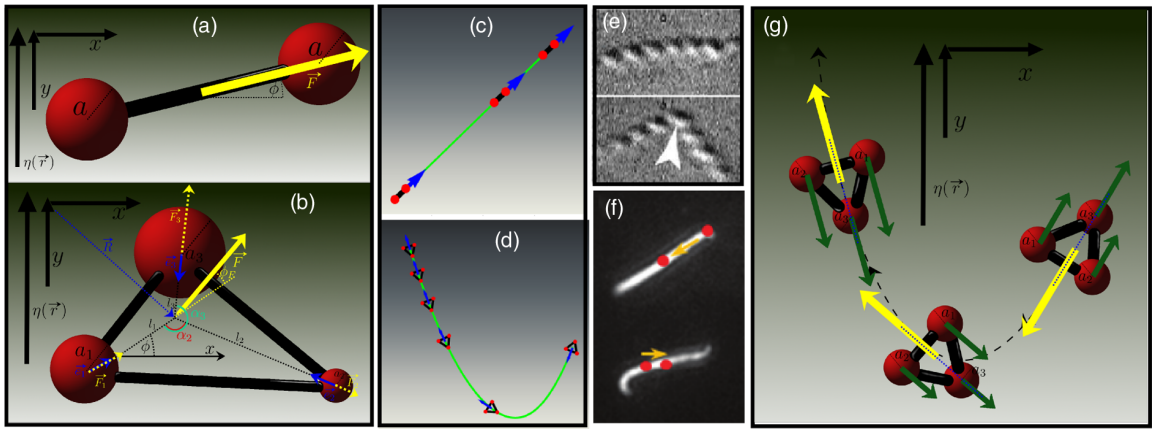

FIG. 2. Viscotaxis in linear swimmers. (a) Uniaxial swimmers do not show viscotaxis and move in the direction of their initial orientation [typical trajectory obtained by solving Eqs. (1) and (2) numerically in arbitrary units shown in (c)]. (b) Nonuniaxial swimmers generically show viscotaxis which is always positive for linear swimmers [typical trajectory in (d)]. (e) *Spiroplasma* and (f) *Leptospira* bacteria changing their body shape from roughly uniaxial to nonuniaxial shapes (snapshots from Refs. [35,39]). (g) Mechanism of viscotaxis. The viscous drag acting on body parts at high viscosity (sphere 1) dominates the drag acting on spheres at low viscosity (sphere 2), which turns the swimmer up the gradient.

with the swimmer in the laboratory frame. Formally, the dynamics of active swimmers therefore still follows Eqs. (1) and (2), but with forces $\mathbf{F}_i \to \mathbf{F}_i(\phi)$, depending on the angle ϕ between the x axis and the axis connecting sphere 1 and $\mathbf{R}$ [see Fig. 2(b)].

Minimal design of viscotactic swimmers.—Let us focus on viscotaxis in linear swimmers and disregard chiral swimmers for now. Accordingly, we only allow for effective forces $\mathbf{F}_i \| (\mathbf{r}_i - \mathbf{R}) =: \mathbf{x}_i$ [57], which sum up to a single force $\mathbf{F}$ pointing at some fixed angle ϕ_F relative to the swimmer [see Fig. 2(b)], i.e., $\mathbf{F}/|\mathbf{F}| = (\cos(\phi + \phi_F), \sin(\phi + \phi_F))$. (Note that any net force acting on a point of the swimmer distinct from $\mathbf{R}$ would indeed create chirality).

We now seek the minimal design of a viscotactic swimmer. Clearly, for a single sphere we have $\mathbf{r}_1 = \mathbf{R}$, such that Eq. (2) is identically fulfilled and the sphere does not change its initial direction of motion. The next simplest candidate, a dumbbell with a propulsion force pointing along the symmetry axis connecting both spheres [Fig. 2(a)], experiences only viscous forces along its symmetry axis but no viscous torque, as $\mathbf{F} = \mathbf{F}_1 + \mathbf{F}_2$ and $\mathbf{x}_{1,2}$ all point along the symmetry axis of the dumbbell [compare Eq. (2) and Fig. 2(c)]. Following this argument, uniaxial swimmers, i.e. swimmers which are symmetric to the axis connecting the beads, cannot show viscotaxis (see also movie 2 in the SM [45]). [This result remains true in three dimensions, of course, and, as we show based on a perturbative solution of the Stokes equation in the presence of a viscosity gradient in the SM [45], it is robust against hydrodynamic far-field interactions up to terms on the order of the relative change of viscosity on the scale of a single bead $a\lambda/\eta(\mathbf{R})$.] To see if triangular swimmers, as the simplest remaining candidate, can show viscotaxis, we now numerically solve Eqs. (1) and (2) for a regular triangular swimmer [Fig. 2(b)] with $a_1 = a_2 = a_3$, $l_1 = l_2 = l_3$, and $\phi_F = 0$. When the swimmer is initialized such that the propulsion forces push it up the viscosity gradient, it continues swimming in this direction. However, when we initialize it such that it starts swimming down the gradient, remarkably, we observe that the swimmer slowly turns and finally approaches a direction leading, again, to motion up the gradient [see Fig. 2(d) and movies 3(a) and 3(b) in the SM [45]]. Therefore, suitable body shapes can create viscotaxis. Figure 2(g) illustrates the underlying mechanism: here, for a given $\dot{\mathbf{R}}$, sphere 1 experiences more drag than sphere 2 and moves more slowly ($f_1 > f_2$ for the magnitudes of the friction forces). As a result the swimmer turns up the gradient until torque balance between the two spheres is reached. Once the swimmer has reached its late-time orientation, the active force points in a constant direction [vertically upwards for the regular triangular swimmer in Fig. 2(g)] and we encounter the same universal $\sqrt{t}$ law as for passive particles in an external force field. These arguments should apply analogously in three dimensions, of course.

Repeating the numerical solution of Eqs. (1) and (2) for other, less regular swimmers, we always find viscoattraction. To see how representative this result is for arbitrarily complicated swimmers, we next develop a systematic theory for viscotaxis.

Theory of viscotaxis.—To understand viscotaxis more generally, we now determine the late-time swimming direction (X_0, Y_0) depending on the swimmer geometry. Here, we first exploit the $\sqrt{t}$ scaling law and use the ansatz $X(t) = X_0\sqrt{t}$, $Y(t) = Y_0\sqrt{t}$ to asymptotically solve Eqs. (1) and (2). As a result (see the SM [45]), we find two possible late-time swimming directions determined by

$$Y_0 = X_0 \tan(\phi_0 + \phi_F), \tag{3}$$

where ϕ_F is fixed by the propulsion forces [Fig. 2(b)] and ϕ_0 is given by

$$\phi_0 = \pm \arctan\left(\sum [c_i \cos(\alpha_i)] \Big/ \sqrt{\sum_{i,j=1}^{N} c_i c_j \cos(\alpha_i - \alpha_j)} \right), \tag{4}$$

with $c_i = a_i l_i^2/(a_1 l_1^2)$ and the angles α_i (with $\alpha_1 = 0$) characterizing the swimmer geometry [see Fig. 1(d)]. The two solutions in Eq. (4) represent fixed points of the orientational dynamics of the swimmer. In fact, depending on the system parameters, one or the other of these solutions accurately agrees with the late-time swimming direction seen in our numerical solutions of Eqs. (1) and (2) (not shown). To predict which of these solutions will attract the swimmer dynamics, we perform a linear stability analysis in the SM [45]. The resulting growth rate of small orientational fluctuations around ϕ_0 reads

$$\sigma = \frac{\sum c_i \sin(\phi_0 - \phi_F + 2\alpha_i)}{2\sin(\phi_0 + \phi_F) \sum c_i}. \tag{5}$$

A ϕ_0 solution is stable if $\sigma < 0$. The remaining task is to find some qualitatively informative relation between the sign of σ in Eq. (5) and the swimmer geometry. Remarkably, it is possible to show [45] that σ is generally negative if $\phi_0 + \phi_F \in (0, \pi)$: that is, we universally find stability of the fixed point [Eq. (4)] representing motion (diagonally) up the viscosity gradient. The conclusion is that, within our model, nonuniaxial linear swimmers generically move up viscosity gradients, no matter what their size and shape may be.

To estimate the role of fluctuations, we compare the typical torque $T_m \sim 6\pi R v L^2 \lambda$ acting on a microswimmer with length $L \sim 10$ μm, speed $v \sim 20$ μm/s (*Leptospira*, *E. coli*), and $R \sim 1$ μm in a waterlike fluid ($\eta \approx 8.9 \times 10^{-10}$ kg/μm s) whose viscosity varies by 5% over L ($\lambda L = 0.05\eta$), with the thermal energy $k_B T$ at $T = 293$ K. This yields $k_B T/T_m \sim 10^{-2}$; i.e., fluctuations are strongly suppressed. The viscotactic alignment time can be estimated as $t_a \sim (L/v)(LF/T_m) = \eta/v\lambda \approx 10$ s, where $FL \sim 6\pi\eta R v L$ acts as a resistive torque opposing T_m. For a triangular synthetic colloid with $L \sim 3\,\mu$m, $R \sim 1$ μm, and $v \sim 3$ μm/s, we find $t_a \sim 30$ s; $k_B T/T_m \sim 0.1$.

Torque-induced negative viscotaxis.—For nonlinear swimmers like circle swimmers or run-and-tumble bacteria, which experience a torque, negative viscotaxis is no longer forbidden by the above results. In fact, this class of swimmers can show both positive and negative viscotaxis. To see this in detail, we reconsider our dumbbell swimmer but now allow the force to point at a finite angle to the swimmer axis [Fig. 3(a)]. Numerically solving Eqs. (1) and (2) for dumbbells swimming with the forcing sphere ahead, we generically observe a spiraling motion up the viscosity gradient [see Fig. 3(b) and movie 4 in the SM [45]], i.e., effectively, viscoattraction. Remarkably, however, dumbbells swimming with the forcing sphere in the back typically spiral down the gradient and effectively show viscorepulsion [see Fig. 3(c) and movie 5 in the SM [45]].

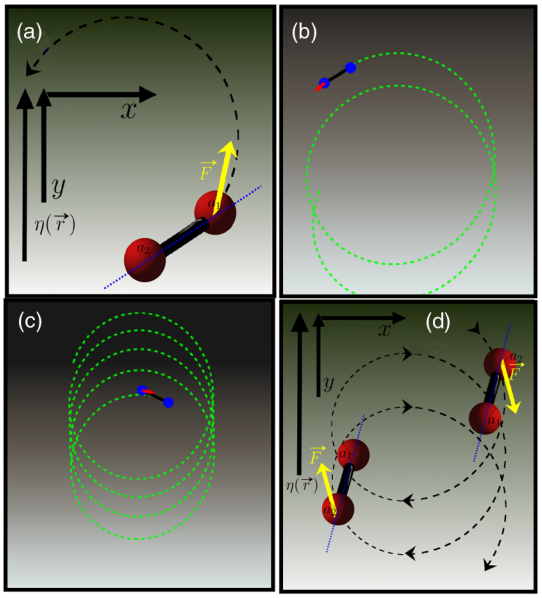

FIG. 3. (a) Viscotaxis in chiral swimmers can be (b) positive [typical trajectory obtained by solving Eqs. (1) and (2) numerically in arbitrary units] or (c) negative. Negative viscotaxis emerges from the fact that (c),(d) back-driven swimmers move faster down the gradient than upwards and systematically overshoot down the gradient while circling (see the text for details).

Physically, from the viewpoint of the forcing sphere, the second sphere provides more additional drag when the dumbbell moves up the viscosity gradient than when moving down the gradient [Fig. 3(d)]. Therefore, the dumbbell swims faster down the gradient and overshoots in this direction within each circle. The inverse situation applies to a dumbbell moving with the forcing sphere ahead [Fig. 3(b)].

Biological implications.—Both *Leptospira interrogans* [33–35] and *Spiroplasma* bacteria [32] show viscoattraction based on a mechanism which is still unclear [35]. Interestingly, the characteristic motility modes of both bacteria contain conformational body changes involving sequences of uniaxial and nonuniaxial shapes; i.e., following the present theory, they should be automatically viscoattractive (rather than requiring speculative viscoreceptors [36]). In fact, without viscotaxis both bacteria would statistically drift to low viscosity regions [36], where they swim poorly. Thus, conformational body deformations in *Leptospira* and *Spiroplasma* might have an unrecognized functionality: to continuously align them towards viscosity regions where they are efficient swimmers.

Conversely, nonlinear swimmers like run-and-tumble bacteria, propelled by flagella in their back, might swim

more effectively during runs pointing down the gradient than during upward pointing runs, similar to the above-discussed chiral dumbbell, which might drive their viscorepulsive behavior [36].

Conclusions.—Nonuniaxial body shapes create viscotaxis, which is generally positive in linear swimmers and effective even for very weak gradients. This generic finding might explain the classical observations of positive viscotaxis seen in *Spiroplasma* and *Leptospira* bacteria; in particular, it suggests that the transitions between uniaxial and nonuniaxial body shapes shown by both microorganisms, previously attributed only to the propulsion mode of these microorganisms, may have an additional functionality: to prevent them from drifting towards regions where they swim poorly. Here, viscotaxis emerges from a generic mechanism hinging on a systematic imbalance of viscous forces acting on the individual body parts of a swimmer. The same mechanism should apply to synthetic swimmers and may serve as a design principle, e.g., for targeted drug delivery to regions of high viscosity.

H. L. acknowledges funding from the SPP 1726 of the Deutsche Forschungsgemeinschaft (DFG, German Research Foundation). B. t. H. gratefully acknowledges financial support through a Postdoctoral Research Fellowship from the Deutsche Forschungsgemeinschaft: HA 8020/1-1. We thank A. M. Menzel and A. N. Morozov for the useful discussions.

*liebchen@hhu.de

[1] D. B. Dusenbery, *Living at Micro Scale* (Harvard University Press, Cambridge, MA, 2009).
[2] M. Eisenbach, *Chemotaxis* (Imperial College Press, London, 2004).
[3] Y. Hong, N. M. K. Blackman, N. D. Kopp, A. Sen, and D. Velegol, Phys. Rev. Lett. **99**, 178103 (2007).
[4] O. Pohl and H. Stark, Phys. Rev. Lett. **112**, 238303 (2014).
[5] S. Saha, R. Golestanian, and S. Ramaswamy, Phys. Rev. E **89**, 062316 (2014).
[6] B. Liebchen, D. Marenduzzo, I. Pagonabarraga, and M. E. Cates, Phys. Rev. Lett. **115**, 258301 (2015).
[7] B. Liebchen, M. E. Cates, and D. Marenduzzo, Soft Matter **12**, 7259 (2016).
[8] B. Liebchen, D. Marenduzzo, and M. E. Cates, Phys. Rev. Lett. **118**, 268001 (2017).
[9] C. Jin, C. Krüger, and C. C. Maass, Proc. Natl. Acad. Sci. U.S.A. **114**, 5089 (2017).
[10] P. Illien, R. Golestanian, and A. Sen, Chem. Soc. Rev. **46**, 5508 (2017).
[11] P. Romanczuk, M. Bär, W. Ebeling, B. Lindner, and L. Schimansky-Geier, Eur. Phys. J. Spec. Top. **202**, 1 (2012).
[12] J. Elgeti, R. G. Winkler, and G. Gompper, Rep. Prog. Phys. **78**, 056601 (2015).
[13] C. Bechinger, R. Di Leonardo, H. Löwen, C. Reichhardt, G. Volpe, and G. Volpe, Rev. Mod. Phys. **88**, 045006 (2016).
[14] G. Jékely, J. Colombelli, H. Hausen, K. Guy, E. Stelzer, F. Nédélec, and D. Arendt, Nature (London) **456**, 395 (2008).
[15] R. R. Bennett and R. Golestanian, J. R. Soc. Interface **12**, 20141164 (2015).
[16] A. Giometto, F. Altermatt, A. Maritan, R. Stocker, and A. Rinaldo, Proc. Natl. Acad. Sci. U.S.A. **112**, 7045 (2015).
[17] C. Lozano, B. ten Hagen, H. Löwen, and C. Bechinger, Nat. Commun. **7**, 12828 (2016).
[18] B. Dai, J. Wang, Z. Xiong, X. Zhan, W. Dai, C.-C. Li, S.-P. Feng, and J. Tang, Nat. Nanotechnol. **11**, 1087 (2016).
[19] S. Klumpp and D. Faivre, Eur. Phys. J. Spec. Top. **225**, 2173 (2016).
[20] J.-F. Rupprecht, N. Waisbord, C. Ybert, C. Cottin-Bizonne, and L. Bocquet, Phys. Rev. Lett. **116**, 168101 (2016).
[21] N. Waisbord, C. T. Lefèvre, L. Bocquet, C. Ybert, and C. Cottin-Bizonne, Phys. Rev. Fluids **1**, 053203 (2016).
[22] A. Bahat, I. Tur-Kaspa, A. Gakamsky, L. C. Giojalas, H. Breitbart, and M. Eisenbach, Nat. Med. **9**, 149 (2003).
[23] Y. Li, Y. Zhao, X. Huang, X. Lin, Y. Guo, D. Wang, C. Li, and D. Wang, PLoS One **8**, e77779 (2013).
[24] A. P. Bregulla and F. Cichos, Proc. SPIE Int. Soc. Opt. Eng. **9922**, 99221L (2016).
[25] T. Bickel, G. Zecua, and A. Würger, Phys. Rev. E **89**, 050303(R) (2014).
[26] P. R. Richter, M. Schuster, M. Lebert, C. Streb, and D.-P. Häder, Adv. Space Res. **39**, 1218 (2007).
[27] A. M. Roberts, J. Exp. Biol. **213**, 4158 (2010).
[28] B. ten Hagen, F. Kümmel, R. Wittkowski, D. Takagi, H. Löwen, and C. Bechinger, Nat. Commun. **5**, 4829 (2014).
[29] A. I. Campbell and S. J. Ebbens, Langmuir **29**, 14066 (2013).
[30] A. I. Campbell, R. Wittkowski, B. ten Hagen, H. Löwen, and S. J. Ebbens, J. Chem. Phys. **147**, 084905 (2017).
[31] K. Wolff, A. M. Hahn, and H. Stark, Eur. Phys. J. E **36**, 43 (2013).
[32] M. J. Daniels, J. M. Longland, and J. Gilbart, Microbiology **118**, 429 (1980).
[33] G. E. Kaiser and R. N. Doetsch, Nature (London) **255**, 656 (1975).
[34] M. G. Petrino and R. N. Doetsch, Microbiology **109**, 113 (1978).
[35] K. Takabe, H. Tahara, M. S. Islam, S. Affroze, S. Kudo, and S. Nakamura, Microbiology **163**, 153 (2017).
[36] M. Y. Sherman, E. O. Timkina, and A. N. Glagolev, FEMS Microbiol. Lett. **13**, 137 (1982).
[37] R. E. Davis and J. F. Worley, Phytopathology **63**, 403 (1973).
[38] R. Gilad, A. Porat, and S. Trachtenberg, Mol. Microbiol. **47**, 657 (2003).
[39] J. W. Shaevitz, J. Y. Lee, and D. A. Fletcher, Cell **122**, 941 (2005).
[40] B. ten Hagen, R. Wittkowski, D. Takagi, F. Kümmel, C. Bechinger, and H. Löwen, J. Phys. Condens. Matter **27**, 194110 (2015).
[41] S. Samin and R. van Roij, Phys. Rev. Lett. **115**, 188305 (2015).
[42] S. C. Takatori and J. F. Brady, Curr. Opin. Colloid Interface Sci. **21**, 24 (2016).
[43] P. Malgaretti, M. N. Popescu, and S. Dietrich, Soft Matter **12**, 4007 (2016).

[44] Power-law profiles $\eta(y) \propto y^n$, for example, lead to $Y^n \dot{Y} = (d/dt) Y^{n+1}/(n+1)$, resulting in $Y(t) \propto t^{1/(n+1)}$, and exponential profiles $\eta(y) \propto e^{\alpha y}$ lead to $Y(t) \propto \ln(t)$, resembling the slowdown in linear profiles.
[45] See Supplemental Material at http://link.aps.org/supplemental/10.1103/PhysRevLett.120.208002, which includes Refs. [46–51], for details of the linear stability analysis and hydrodynamic considerations.
[46] A. Najafi and R. Golestanian, Phys. Rev. E **69**, 062901 (2004).
[47] K. Pickl, J. Götz, K. Iglberger, J. Pande, K. Mecke, A.-S. Smith, and U. Rüde, J. Comput. Sci. **3**, 374 (2012).
[48] J. Pande and A.-S. Smith, Soft Matter **11**, 2364 (2015).
[49] J. E. Avron, O. Kenneth, and D. H. Oaknin, New J. Phys. **7**, 234 (2005).
[50] G. Grosjean, M. Hubert, G. Lagubeau, and N. Vandewalle, Phys. Rev. E **94**, 021101(R) (2016).
[51] J. S. Guasto, K. A. Johnson, and J. P. Gollub, Phys. Rev. Lett. **105**, 168102 (2010).
[52] D. J. Earl, C. M. Pooley, J. F. Ryder, I. Bredberg, and J. M. Yeomans, J. Chem. Phys. **126**, 064703 (2007).
[53] J. Dunstan, G. Miño, E. Clement, and R. Soto, Phys. Fluids **24**, 011901 (2012).
[54] A. Farutin, T. Piasecki, A. M. Słowicka, C. Misbah, E. Wajnryb, and M. L. Ekiel-Jeżewska, Soft Matter **12**, 7307 (2016).
[55] H. R. Vutukuri, B. Bet, R. van Roij, M. Dijkstra, and W. T. S. Huck, Sci. Rep. **7**, 16758 (2017).
[56] B. ten Hagen, S. van Teeffelen, and H. Löwen, J. Phys. Condens. Matter **23**, 194119 (2011).
[57] Forces not parallel to $\mathbf{r}_i - \mathbf{R}$ (i) produce torques which can generically not be canceled by viscous torques, as the latter ones depend on the speed of the swimmer, whose $\sqrt{t}$ time dependence in turn forbids a permanent canceling, and (ii) cases where torques originating from different forces cancel each other out do not create any new physics and can be disregarded.